Effect of substrate temperature on the structural, optical, electrical, and morphological properties of zinc oxide thin films

S Dif [1], S Benramache [1], A Ammari [2,3] and A Gahtar [4*]

1. Department of Materials Sciences, Faculty of Sciences, University of Biskra, Algeria
2. Department of Physics, Faculty of Matter Sciences, University of Tiaret, Algeria
3. Laboratory of Micro and Nanophysics (LaMiN), National Polytechnic School of Oran (ENPO), Oran, Algeria
4. Department of Biology, Faculty of Sciences, University of Hamma Lakhdar, El Oued, Algeria

E-mail: abdelouahab-gahtar@univ-eloued.dz

Abstract

The present paper reports on the effect of substrate temperature on the physical properties of zinc oxide (ZnO) thin films deposited using spray-pyrolysis technique. The films exhibit a polycrystalline nature with a preferred orientation along [002]. Furthermore, the average crystallites size increases with increasing the substrate temperature. The scanning electron microscopy results showed that the films were evenly distributed and homogeneous. The average optical transmittance varies in the range of 62 to 90% depending on the substrate temperature. On the other hand, with increasing the substrate temperature, the absorption coefficient decreases and the optical band gap varies in the range of 3.25 - 3.28 eV. The electrical conductivity of films varies between 18 and 58 mS.cm^{-1}.

Keywords: ZnO thin films; substrate temperature, spray-pyrolysis; morphology, optical band gap; electrical conductivity

1. Introduction

Among optical materials, ZnO thin films are the most attractive of solar cell applications and microelectronic and they have been the subject of extensive studie [1, 2]. In addition, the piezoelectric properties of ZnO are suitable for surface acoustic wave (SAW) devices, ultrasonic transducers and sensors [3]. The transparent conductive ZnO thin films are widely used in light emitting diodes, anti-reflective coatings [4], transparent electrodes in solar cells [5], gas sensors [6], varistors [7], spintronics devices and lasers [8]. ZnO crystalizes in the hexagonal structure (wurtzite type), which favorites the growth of high quality epitaxial oriented thin films. In this structure, each Zn atom is tetrahedral coordinated with four O atoms and the electrons of zinc hybridizes with the p-electrons of oxygen [8]. Therefore, the electronic structure of the material yiels a wide direct band gap of 3.3 eV [9], high exciton binding energy (60 MeV [10]), high emission, high saturation speed (3.2×10^7 cms^{-1}) and high breakdown voltage [11] and high mobility [12]. Numerous techniques were successfully applied to deposit high quality of ZnO thin films such as chemical vapor deposition (CVD) [13], molecular beam epitaxy (MBE) [14], electrochemical deposition [15], pulsed laser deposition (PLD) [16], magnetron sputtering [17], and sol-gel techniques [18]. However, the spray-pyrolysis technique is most convenient due to its low cost and easy processing [19]. Commonly, the films deposited with this technique are highly transparent and conductive.

The present study investigates the influence of the substrate temperature on the physical properties of ZnO thin films deposited using the spray-pyrolysis technique.

2. Experimental details

2. 1. ZnO synthesis

The precursor solution consisted of acetate zinc hyxahydrate (Zn(NO$_3$)$_2$.6H$_2$O) dissolved in 100 ml of ionized water (0.1 mol/l) under stirring at 70 °C. A few drops of HCl were added to the above solution to enhance the solubility of the precursor. Finally, a transparent and clear solution was obtained. The films were deposited on glass substrates (2×7 cm^2) by spray-pyrolysis technique at different substrate temperatures (325, 350, 375, and 400 °C). The distance between the substrates and the spray gun nozzle was fixed at 30 cm. The ambient air was used as a gas vector with a flow rate of 7 ml/min. The spray gun of the nebulizer is connected
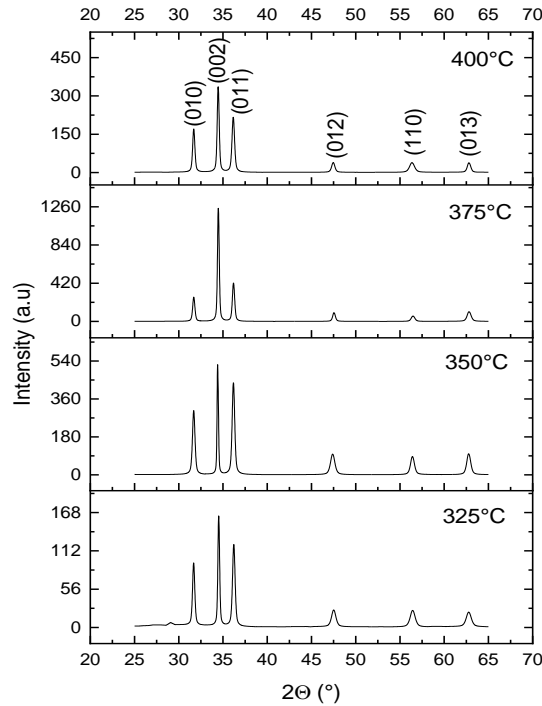
Figure 1. X-ray patterns of ZnO thin films deposited at different substrate temperatures (325, 350, 375, and 400 °C).

to a manually operated stepper motor to control the position of the spray in the plane (X,Y). After deposition, the films were slowly cooled down to room temperature under ambient air.

The film thickness was estimated using the weight method, which yields the thickness acoording to the formula [20]:

$$t = \frac{m}{\rho \times S},\qquad(1)$$

where t is thickness of the film, m is mass deposited on the substrate, S is the area of the film and ρ is the density of ZnO (5.675 g/cm^3[21]).

2. 2. Characterization

The structural analysis was carried out using an X-ray diffractometer (DRX; Mini Flex-Rigaku) with a Cu-K$_\alpha$ radiation (λ= 1.5418 Å) in the range of 20 − 60°, using the Brentano-Bragg geometry. The morphology of the surface was analyzed using a scanning electron microscope (SEM; Qanta 350) equipped with an energy dispersive spectrometer (EDS) for elementary analysis. A dual-beam UV-visible spectrophotometer (UV-3101; Shimadzu), was used to measure the transmittance and absorbance in the wavelength range of 300 − 1100 nm with a resolution of 5 nm. The electrical conductivity of the films was measured in a coplanar structure obtained with evaporation of four golden stripes on film surface. All the analysis were conducted on the films without thermal treatment after deposition.

3. Results and Discussions
3. 1. X-Ray Diffraction

Figure 1 shows the XRD patterns of ZnO thin films. Six

diffraction peaks are observed at 2θ = 31.7°, 34.4°, 36.1°, 47.4°, 53.3° and 62.7°. Theses Bragg reflections are attributed to the following planes (010), (002), (011), (012), (110) and (013), respectively. The data also depict the polycrystalline nature of the films and correspond to the Wurtzite structure (hexagonal) of ZnO according to the JCPDS card # 98-006-5121 (space group P63mc; N° = 186). Furthermore, it is observed that the film deposited at 375 °C has a higher and narrow diffraction peak suggesting a better crystallinity compared to the other films.

The inter-planes distance (d_{hkl}) was calculated using Bragg formula [22] .

$$2d_{hkl} \sin\theta = n\lambda,\qquad(2)$$

The unit cell parameters a, b and c, were determined using the following formula [23]:

$$1/(d_h kl^2) = 3/4((h^2 + k^2 + hk)/a^2) + l^2/c^2\qquad(3)$$

The unit cell volume was determined using the following formula:

$$V = a^2 \times c \times \sin(60°),\qquad(4)$$

Table 1 summarizes the obtained values of a, b, c and V for different substrate temperatures. It is observed that the ratio (c/a) nearby 1.6 determined for our samples is slightly larger than the standard value (1.59) of the hexagonal structure. This may be due to vacancies that cause local changes and contraction of the lattice.

The texture coefficient (TC$_{hkl}$), which is calculated in terms of the intensity of each orientation (I$_{hkl}$) to the corresponding intensity of the JCPDS card (I$_{0hkl}$), gives information on the probability of the growth according to the orientation [hkl]. This coefficient is given by [24]:

Table 1. Lattice parameters (a. b and c) compared to the JCPDS card.

Substrate temperature	Latice parameters						Unit cell volume (Å^3)
	Our data			JCPDS card #98-006-5122			
	a=b (Å)	c (Å)	c/a	a=b (Å)	c (Å)	c/a	
325 °C	3.263	5.236	1.605				47.944
350 °C	3.259	5.226	1.604	3.265	5.219	1.598	47.735
375 °C	3.254	5.239	1.610				47.707
400 °C	3.257	5.224	1.604				47.658

Table 2. Structurales parameters of ZnO thin films (d_{hkl}: Bragg distance. TC_{hkl} : Texture coefficient. D_{hkl}: Crystallites size. δ_{hkl} : Dislocation density. and ε_{hkl} : Micro-stress).

Substrate temperature	(hkl)	d_{hkl} (Å)	TC_{hkl}	D_{hkl} (nm)	δ_{hkl} (10^{15} lines/m^2)	ε_{hkl} (10^{-3})
	010	282	1.209	32.137	0.968	4.240
	002	259	2.287	45.320	0.486	2.766
325 °C	011	248	1.588	28.457	1.234	4.205
	012	191	0.318	16.887	3.506	5.467
	110	163	0.315	15.344	4.247	5.126
	013	148	0.280	15.836	3.987	4.509
	010	282	1.099	28.116	1.264	4.845
	002	260	2.252	64.704	0.238	1.943
350 °C	011	248	1.602	28.453	1.235	4.210
	012	191	0.350	16.879	3.509	5.483
	110	163	0.319	20.459	2.389	3.846
	013	148	0.376	21.117	2.242	3.381
	010	282	0.695	32.138	0.968	4.238
	002	260	3.485	45.314	0.486	2.770
375 °C	011	248	1.115	32.524	0.945	3.682
	012	191	0.260	29.552	1.145	3.122
	110	162	0.157	22.322	2.006	3.521
	013	147	0.284	21.122	2.241	3.379
	010	282	1.202	32.138	0.968	4.238
	002	260	2.451	37.754	0.701	3.326
400 °C	011	248	1.523	28.452	1.235	4.212
	012	191	0.273	23.635	1.790	3.91
	110	163	0.264	15.339	4.250	5.134
	013	147	0.283	25.344	1.556	2.81

$$TC_h kl = (I_h kl / I_\circ hkl) / (N^{(-\backslash)}[\sum\nolimits_{(i=\backslash)}^{n} I_h kl / I_\circ hkl]) \quad (5)$$

where N is the number of diffraction peaks. The obtained values of TC_{hkl} are gathered in table 2. It is observed that the value of the greater texture coefficient corresponds to the plane (002), indicating a preferred orientation. Hence, the peak (002) has the highest intensity when compared to the other peaks and the growth of the films occurs parallel to the substrate.

The crystallites size (D) was estimated for all diffraction peaks using Debye formula [25]:

$$D = \frac{k \times l}{\beta_{1/2} \cos\theta}, \quad (6)$$

where k is a constant (k = 0.90), $\beta_{1/2}$ is the full width at half the maximum of the diffraction peak, θ is the Bragg angle for each plane (hkl), and $\lambda = 1.5406\,\text{Å}$ is the wavelength of the X-ray radiation.

The dislocation density (δ_{hkl}), which measures the amount of defects in a crystal is defined as the length of dislocation lines per unit of volume. It was determined using the following formula [26]:

$$\delta_{hkl} = 1/(D^2_{hkl}), \quad (7)$$

On the other hand, the microstrain (ε_{hkl}), was estimated using the following formula [27]:

$$\varepsilon_{hkl} = \frac{\beta_{1/2}}{4\tan\theta}, \quad (8)$$

The obtained values of δ_{hkl} and ε_{hkl} for each plane are gathered in table 2. The average crystallites size $<D>$, micro-stress $<\varepsilon>$ and the dislocation density $<\delta>$ can be determined using the texture coefficient according to the formulas [23,28,29]:

$$\prec D \succ = \frac{\sum TC_{hkl} \times D_{hkl}}{n}, \quad (9)$$

$$\prec \varepsilon \succ = \frac{\sum TC_{hkl} \times \varepsilon_{hkl}}{n}, \quad (10)$$

$$\prec \delta \succ = \frac{\sum TC_{hkl} \times \delta_{hkl}}{\sum TC_{hkl}}, \quad (11)$$

Table 3. Obtained average values of D, ε, and δ of ZnO thin films.

Substrate temperature	$\langle D \rangle$	$\langle \varepsilon \rangle$	$\langle \delta \rangle$ (10^{15} lines/m^2)
325 °C	25.663	4.386	2.405
350 °C	29.955	3.951	1.114
375 °C	30.495	3.452	1.298
400 °C	27.110	3.939	1.750
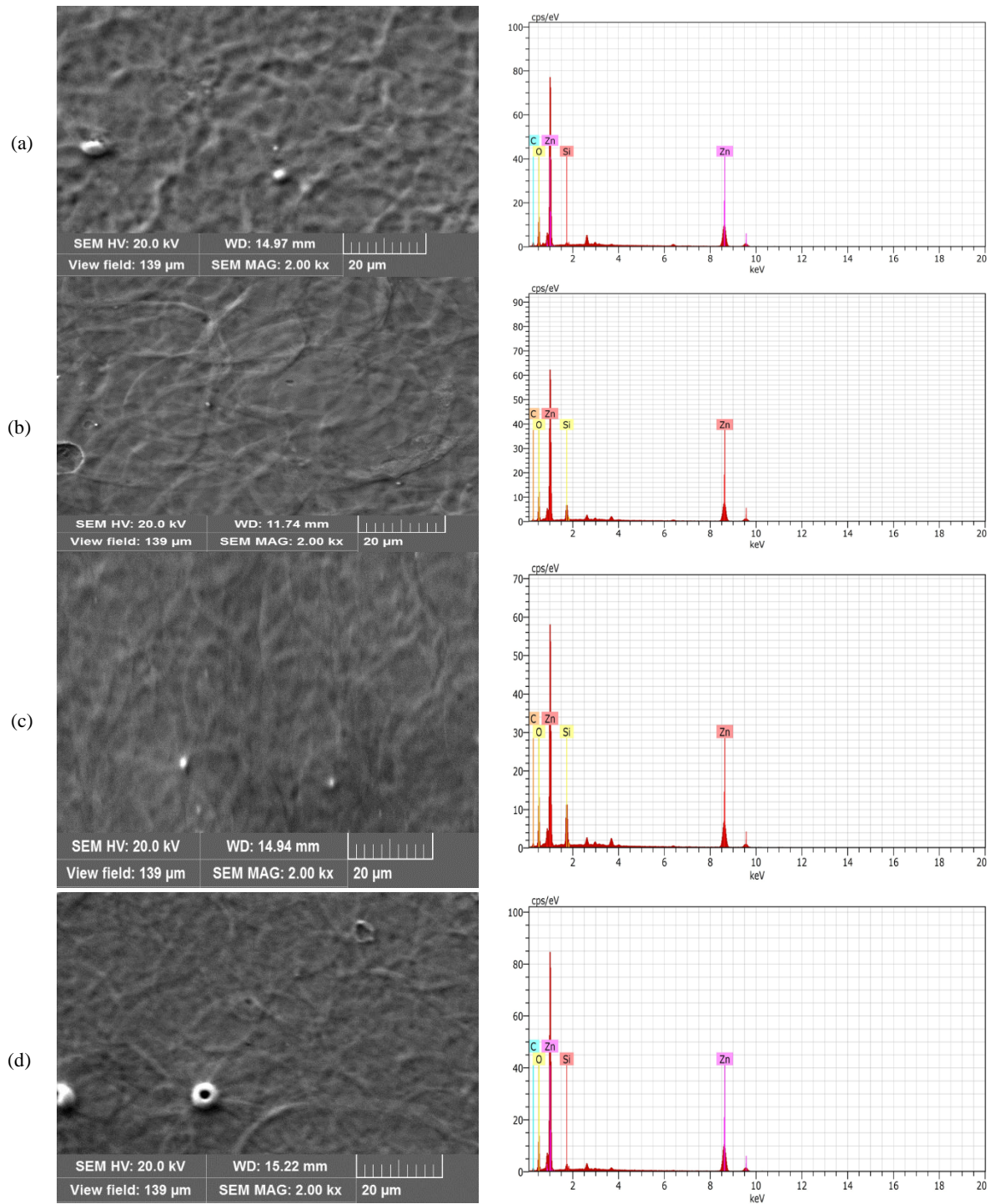
Figure 2. SEM and EDS micrographs of ZnO thin films deposited at different substrate temperatures: a) 325, b) 350, c) 375, and d) 400 °C.

Table 4. Elementary analysis of ZnO thin films.

Substrate temperature	Zn		O	
	at (%)	wt (%)	at (%)	wt (%)
325 °C	31.04	46.34	43.01	15.71
350 °C	29.95	45.87	46.63	17.47
375 °C	24.88	42.29	47.33	19.87
400 °C	34.43	50.94	45.6	16.51
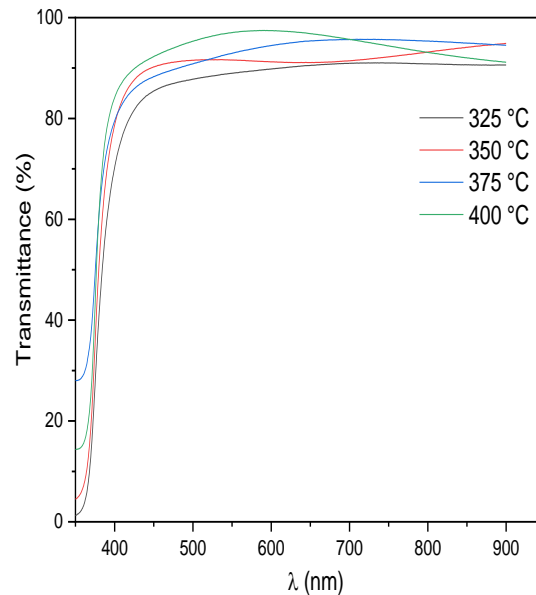
Figure 3. Transmittancy spectra of ZnO thin films deposited at different substrate temperatures (325, 350, 375, and 400 °C).

Table 3 summarizes the values of the above structural parameters. It is evident that the highest crystallites size value and the lowest stress and dislocation density values are obtained for the film deposited at 375 °C. These results are consistent with the results of the texture coefficient above.

3. 2. SEM and EDS analysis
Figure 2 shows the SEM and EDS micrographs of our samples. It was observed that the films are homogeneous, granular and well-deposited on the substrate without any micro-crack. Table 4 resumes the results of the EDS analysis. It is observed that the concentration of Zn element decreases while the concentration of O element increases with increasing the substrate temperature. Thus, the oxidation of the surface is enhanced by the increase of the thermal energy. However, it is observed the concentration of Zn is greater for the film deposited at 400 °C, while the concentration of O element slightly deceases compared to the previous ones. This is due to the promoted formation of interstitial Zn in the lattice by the enhancement of the thermal energy.

3. 3. Optical properties
Figure 3 shows the transmittance spectra of the samples. It is observed that the films exhibit a good optical transparency in the visible range ($\lambda > 400$ nm). Furthermore, the average transmittance in this range increases depending on the substrate temperature. Indeed, the average transmittance is 89.8, 92.1, 94.1 and

94.8% for the films deposited at 325, 350, 375, and 400 °C, respectively. On the other hand, the films depicted strong absorption in the ultraviolet range. The optical absorption coefficient (α) was calculated from transmittance using the relation :

$$\alpha = \frac{1}{t}\log(\frac{1}{T}), \tag{12}$$

where T is the transmittance and t is the thickness of the films. Therefore, the optical band gap of the samples was determined in this range using Tauc plots according to the following dependence [25] :

$$(\alpha h\nu)^2 = A(h\nu - E_g), \tag{13}$$

where α is the absorption coefficient, $h\nu$ photon energy, A a constant, and E_g is the band gap. Figure 4 shows the plots $(\alpha h\nu)^2$ versus $h\nu$. The value of the optical band gap is deduced by extrapolation of the linear part to the energy axis. Table 5 summarizes the obtained values. It is observed that the E_g varies slightly with the substrate temperature. In addition, these values are close to the reported ones for this material in literature [30-33].

3. 4. Electrical conductivity
Figure 5 shows the variation in the electrical conductivity of the films versus the substrate temperature. It is observed that the conductivity of the films increases from 18 to 58 mS.cm^{-1}, and then decreases to 43 mS.cm^{-1}. The enhancement of the conductivity is due to reduced disorder and better crystallinity in the films with the increase of the growth
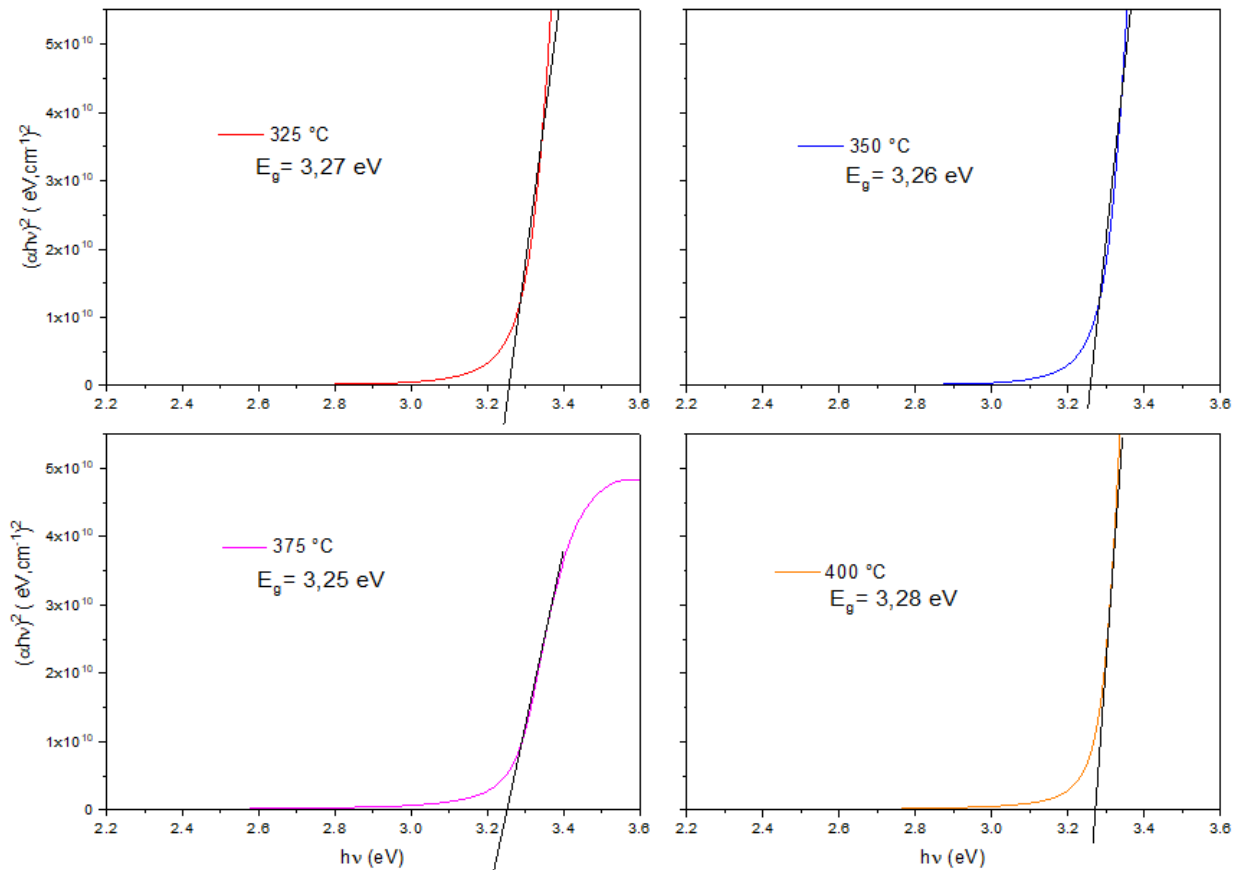
Figure 4. Tauc plots $(\alpha h\nu)^2$ vs. $h\nu$ of ZnO thin films deposited at different substrate temperatures (325, 350, 375, and 400 °C).
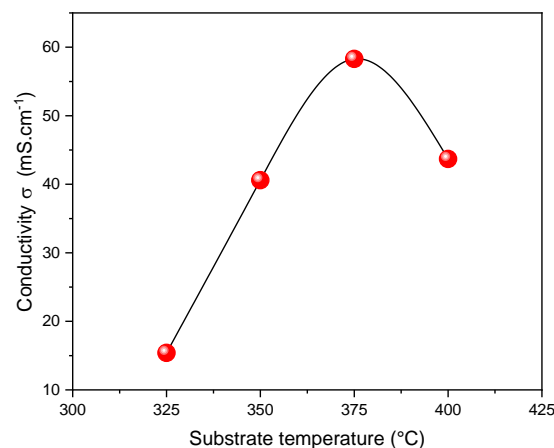

Figure 5. Electrical conductivity of ZnO thin films versus substrate temperature.

temperature i.e. substrate temperature. On the other hand, the observed decrease for the film deposited at 400 °C, may be due to the change in the density of the free carriers and reduced mobility [37]. The electronic defects such as interstitial Zn and oxygen vacancies strongly influence the charge transport in the films [38].

4. Conclusions

Highly transparent conductive thin films of zinc oxide were deposited by spray-pyrolysis technique, at different substrate temperature. The results revealed that the films are polycrystalline and crystalizes along [002]. The average crystallites size varies from 25.6 to 30.5 nm, depending on the growth temperature. The analysis of the morphology displayed that the films are homogenous without any micro-cracks. The elementary analysis showed that the stoichiometry of the films varies depending on the temperature of deposition. The electrical conductivity of the samples varied in the range of 18 – 58 mS.cm^{-1}, which the highest values was recorded for the films deposited at 375 °C.

References

1. P E Agbo and M N Nnabuchi, *Chalcogenide Lett.* **8** (2011) 273.
2. F Atay, *et al.*, *Turk. J. Phys.* **27** (2003) 285.
3. Z B Bahşi and A Y Oral, *Opt. Mater.* **29** (2007) 672.
4. M Baradaran, *et al.*, *J. Alloys Compd.* **788** (2019) 289.
5. S Benramache, et al., *J. Semicond.* **34** (2013) 113001.
6. R Boughalmi, *et al.*, *Mater. Sci. Semicond. Process.* **26** (2014) 593.
7. R Boughalmi, *et al.*, *Mate. Chem. Physic.* **163** (2015) 99.
8. A Boukhachem, *et al.*, *Sens. Actuators* A*: Phys.* **253** (2017) 198.
9. S H Cho, *Trans. Electr. Electron. Mater.* **10** (2009) 185.
10. B D Cullity, "*Elements of X-ray Diffraction*", Addison-Wesley Publishing, (1956).
11. A Gahtar, *et al.*, *Adv. Mater. Sci.* **20** (2020) 36.
12. A Gahtar, *et al.*, *Chalcogenide Lett.* **19** (2022) 103.
13. A Gahtar, *et al.*, *Inorg. Nano-Metal Chem.* **52** (2022) 112.
14. A Goktas, *et al.*, *J. Alloys Compd.* **893** (2022) 162334.
15. A Hafdallah, *et al.*, *J. Alloys Compod.* **509** (2011) 7267.
16. Y Huang, *et al.*, *J. Mater. Chem.* C **8**(2020) 12240.
17. M R Islam, *et al.*, *Surf. Interfaces* **16** (2019) 120.
18. A Jiamprasertboon, *et al.*, *ACS Appl. Electro. Mater.* **1** (2019), 1408.
19. R Karthikeyan, *Doctoral Dissertation Thesis*, Shizuoka University (2015).
20. L H Kathwate, *et al.*, *Sens. Actuator.* A*: Phys.* **313** (2020) 112193.
21. H A Kavak, *et al., Vacuum* **83**, 3 (2008) 540.
22. Z N Kayani, F Saleemi, and I Batool, *Appl. Phys.* A **119** (2015) 713.
23. F Khan, W Khan, and S D Kim, *Nanomaterials* **9**, 3 (2019) 440.
24. V Kumar, *et al., Phys.* B*: Condens. Matter* **552** (2019) 221.
25. Y Lu, *et al., Inter. J. Appl. Ceram. Techno.* **17**, 2 (2020) 722.
26. S Marouf, *et al., Mater. Res.* **20** (2016) 88.
27. N Marsi, *et al., Inter. J. Nanoelectronics. Mater.* **13** (2020) 113.
28. P Godse, *et al., J. Surf. Eng. Mater. and Adv. Technol.* **1, 02** (2011) 35.
29. P Prepelita, *et al., Appl. Surf. Sci.* **256**, 6 (2010) 1807.
30. A Rahal, S Benramache, and B Benhaoua, *Eng. J.* **18**, 2 (2014) 81.
31. M Riahi, *et al., Thin Solid Films* **626** (2017) 9.
32. V Sallet, *et al., Nanotechnology* **31**, 38 (2020) 385601.
33. T Shen, *et al., Appl. Phys. Lett.* **120**, 4 (2022) 042105.
34. S S Shinde, *et al., Appl. Surf. Sci.* **258** (2012) 9969.
35. D T Speaks, *Int. J. Mech. Mater. Eng.* **15** (2020) 1.
36. D Vernardou, *et al., J. Crys. Growth* **308** (2007) 105.
37. W Yang, *et al., Ceram. Int.* **46**, 5 (2020), 6605.
38. Z Zhang, *et al., Superlattices and Microstruct.* **49**, 6 (2011) 644.